Journal of Oceanography, Vol. 62, pp. 577 to 586, 2006

Short Contribution

Comparison of Downward Surface Solar Radiation Derived from GMS5/VISSR and of Reanalysis Products

HUILING QIN*, YOSHIMI KAWAI and HIROSHI KAWAMURA

Center for Atmospheric and Oceanic Studies, Graduate School of Science, Tohoku University, Sendai 980-8578, Japan

(Received 25 July 2005; in revised form 17 January 2006; accepted 26 January 2006)

A high-resolution downward surface solar radiation (DSSR) dataset has been produced using geostationary meteorological satellite measurements. Its validation with in situ observations shows that the daily satellite DSSRs are highly accurate. Comparing the satellite DSSRs with reanalysis DSSR datasets, the former has higher probability density in a low value range, and lower density in a high value range. Overestimations of the reanalysis DSSR are significant in the low range. Correlations between the reanalysis DSSRs and the satellite DSSR are relatively low in the tropics. It is suggested that the satellite DSSRs have good potential to capture cloud behavior in the tropics.

Keywords:
· Satellite derived solar radiation,
· GMS,
· validation,
· dataset.

1. Introduction

In the atmosphere-ocean system, shortwave radiation from the sun is absorbed by the ocean and crucial heat energy drives the atmospheric and oceanic motions. Many studies have pointed out that the atmosphere and ocean circulations are very sensitive to the fine structure of the solar radiative heating. Webster and Lukas (1992) mentioned that the heat flux between the ocean and the atmosphere is temporally and spatially complex in the region of active convection where the smallest spatial scale of a convective cell is about 1–10 km. Zhang *et al*. (2004) indicated that a knowledge of radiative flux variations on scales from diurnal and mesoscale to interannual and planetary scale is important to understand how cloud and water vapor variations interact with atmospheric and oceanic circulations. Heretofore, the largest sources of uncertainty appearing in the energy budget are how much shortwave radiation can be absorbed in atmosphere and how much radiation arrives at the surface (Kiehl and Trenberth, 1997).

Although the importance of solar radiative forcing in the air-sea coupled system is well recognized, there are insufficient observations of solar radiation to cover the air-sea interactions on scales from daily to intraseasonal. In particularly, little is known about the variability of the energy budget in air-sea interaction systems with high frequencies and corresponding small scales. Although in situ radiation measurements have been made for decades (e.g., Hanawa and Kizu, 1990; Iwasaka *et al*., 1994), there are few high-resolution solar radiation datasets available for the investigation of such small-scale air-sea interactions.

In order to generate high-resolution solar radiation information for the air-sea interaction studies, scientists have tried to derive downward surface shortwave radiation (DSSR) from satellite observations via physical models (e.g., Gautier *et al*., 1980; Kizu, 1995; Zhang *et al*., 2004). These models incorporate the effects of water vapor, cloud cover, ozone, Rayleigh scattering and aerosols, which greatly influence the amount of shortwave radiation that reaches the earth's surface. Because the DSSR diurnal variation, which mainly results from the earth's autorotation, is the most significant radiation process in the earth system, the visible and infrared observations provided by geostationary meteorological satellites were shown to be quite useful for this purpose (Gautier *et al*., 1980). These observations have high temporal and spatial resolutions of about one hour and several kilometers, respectively.

Kizu (1995) derived DSSR using Geostationary Meteorological Satellites (GMS)-3/Visible Infrared Spin-Scan Radiometer (VISSR) observation data. His model assumed that solar radiation reduced by clouds increased linearly with satellite-measured albedo. Validation of the

* Corresponding author. E-mail: qin@ocean.caos.tohoku.ac.jp

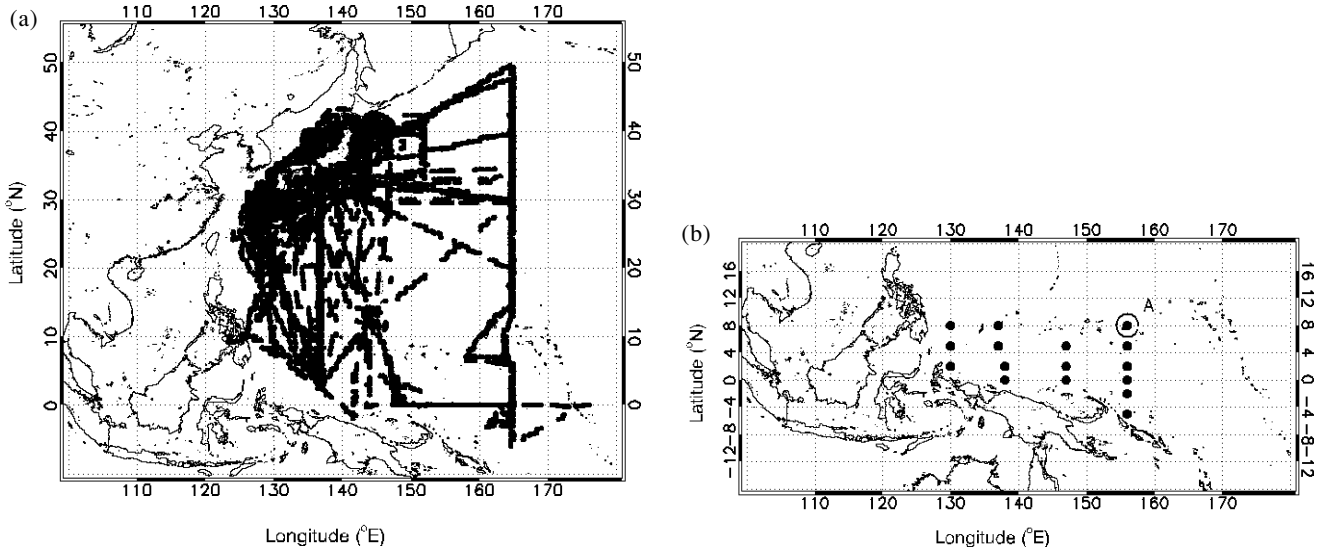

Fig. 1. In situ DSSR observation locations: (a) JMA research vessels in 1996–2003, and (b)TRINTON buoys in 1998–2003.

satellite DSSRs against land-based observations showed at the root-mean-square (RMS) daily and monthly errors were 20% and 10%, respectively. Tanahashi *et al*. (2000) pointed out that DSSR varied rapidly with time when clouds were moved by wind. Tanahashi *et al*. (2001) then improved the cloud absorption coefficient in Kizu's model using their automatic tuning algorithm. Using the Tanahashi *et al*. coefficient, Kawamura *et al*. (1998) successfully estimated DSSR over the sea off Sanriku coast. The RMS of daily DSSR was less than 10%. Kawai and Kawamura (2005) found that the cloud attenuation coefficient for low-albedo cases over the ocean needed to be larger in the low latitudes than used in past research. After improvement, the RMS of the daily mean DSSR over the western and equatorial Pacific was reduced to 11–14%.

Here the high-resolution satellite DSSR dataset has been extended using the coefficient table proposed by Kawai and Kawamura (2005) and 7.5 years of GMS-5/VISSR visible and infrared observational data. This dataset covers temporal scales from diurnal to inter-annual through meso, inter-seasonal, seasonal and annual with a high spatial resolution of 0.05 degree for the GMS coverage, including the western equatorial Pacific. The purpose of this study is to investigate the accuracy and characteristics of the validated high-resolution satellite DSSR, and to compare it with other reanalysis DSSR datasets.

Major operational meteorological agencies have produced historical global objective analysis datasets of atmospheric and oceanic parameters for recent decades with a fixed state-of-the-art numerical weather prediction data assimilation system. During the last two decades, reanalysis DSSR products have been used in a wide range of research, such as large-scale air-sea interaction, global energy budget, climate, etc. In this study, we selected three representative reanalysis DSSR products: the National Center for Environmental Prediction and National Center for Atmospheric Research reanalysis 1 project (NCEP/NCAR 1) DSSR, European Center for Medium-Range Weather Forecasts 40 years Reanalysis Project (ERA40) DSSR, and the Japanese 25-year Reanalysis Project (JRA25) DSSR. Kanamitsu *et al*. (2002) pointed out that the NCEP/NCAR reanalysis 2 data overestimated shortwave radiation than the reanalysis 1 and in situ one by 3% of global annual mean value, while the reanalysis 1 DSSR agreed better with the in situ one. Therefore, we chose the NCEP/NCAR reanalysis 1 daily DSSR for comparison with satellite DSSRs.

Section 2 of this paper introduces the basic information provided for satellite-based, in situ and reanalysis DSSRs. The accuracy/characteristics of the satellite DSSR data are described in Section 3. Section 4 describes results of comparisons between the satellite DSSR and the NCEP/NCAR 1, ERA40 and JRA25 reanalysis datasets. The results are discussed in Section 5 and the conclusions are given in Section 6.

2. Satellite DSSR Dataset and In Situ Data

The satellite DSSR data were derived with Kizu's (1995) model and the coefficient table given by Kawai and Kawamura (2005) for the GMS-5/VISSR measurements. The DSSR data are available from January 1996 to May 2003. The coverage area is from 80°E to 160°W,

Table 1. Basic description of the satellite and the reanalysis DSSRs.

Name	Satellite DSSR	NCEP/NCAR 1	ERA40	JRA25
Generation organization	Caos. Tohoku Univ.	NCEP-NCAR	ECMWF	JMA/CRIEPI
Period	1996.01–2003.05	1948–Present	1957.09–2002.08	1979–2004
Spatial resolution	0.05°×0.05°	Gaussian grids	2.5°×2.5°	2.5°×2.5°
Coverage	80°E–200°E, 60°S–60°N	0–358.13°E, 88.54°S–88.54°N	0–360°E, 90°S–90°N	0–360°E, 90°S–90°N

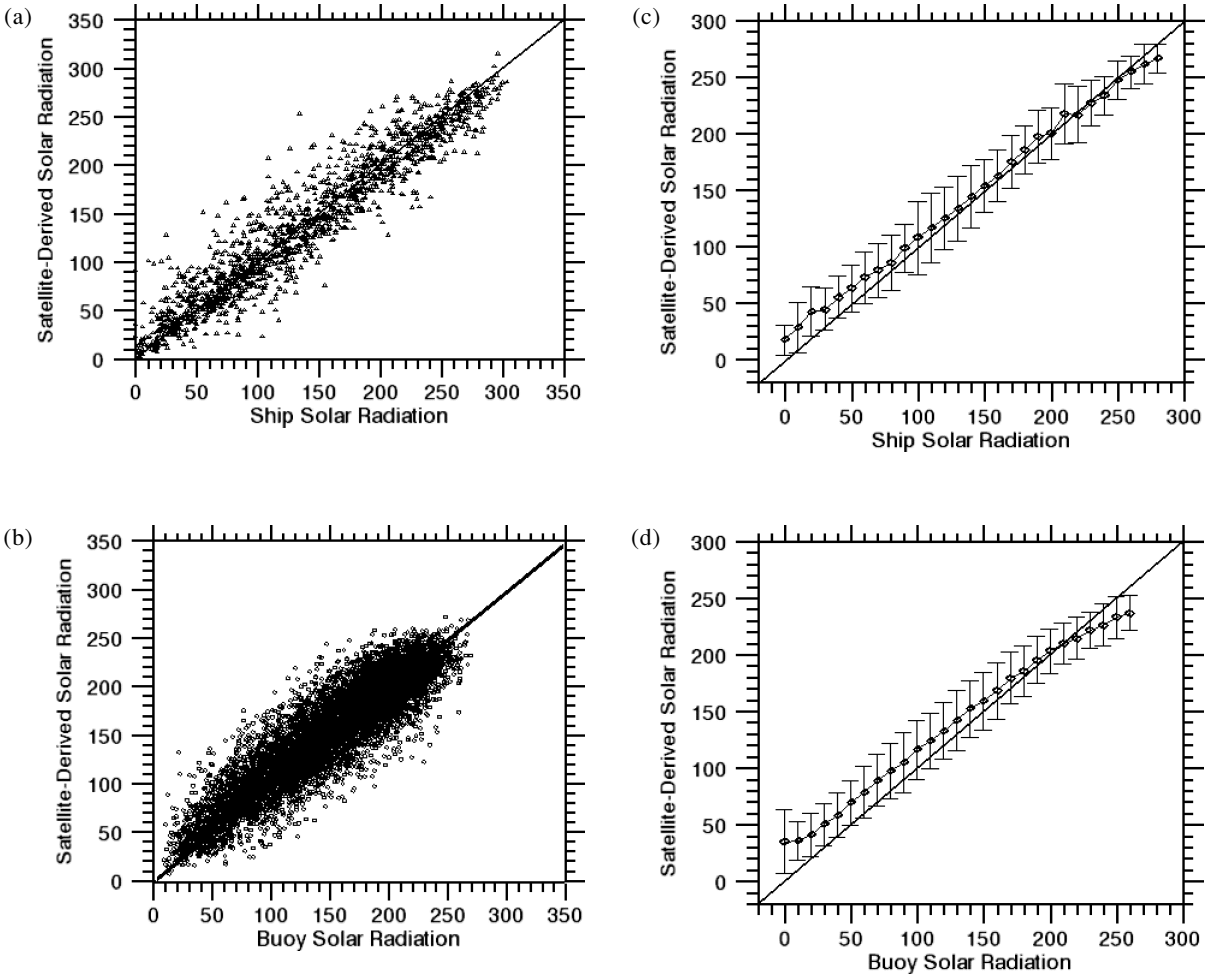

Fig. 2. Comparisons between the satellite daily DSSR and (a) ship data, and (b)buoy data. Unit is W/m^2.

60°S to 60°N with 0.05° × 0.05° spatial resolution. The GMS-5 daytime data were received hourly, 14 times per day. All the available data (38,178 satellite observed scenes) were processed to the hourly satellite DSSR data. Daily mean DSSR were then produced by a simple average of all the hourly DSSRs of every day. The coefficients of Kawai and Kawamura (2005), which are depend on the satellite-measured albedo, solar zenith angle and latitude, significantly improve the accuracy of satellite DSSR over the ocean. The model description and procedure for generating DSSR are documented in Appendix.

The in situ DSSR dataset comprises ship-based observations and Triangle Trans-Ocean buoy Network (TRITON) data. Kawai and Kawamura (2005) described the details of in situ DSSR data spanning 1997–2000, including their spatial distribution and measurement accuracy. Research vessel observational cruises have been carried out by the Japan Meteorological Agency (JMA).

Table 2. Error statistics of the satellite DSSR derived from the GMS-5 VISSR observations. The figures in the lowest row show the statistics from both the ship and buoy match-ups.

Year	Satellite ~ Ship (W/m^2)			Satellite ~ Buoy (W/m^2)		
	No.	Bias	RMS	No.	Bias	RMS
1996	74	20.7	29.7 (18.4%)			
1997	418	4.4	22.3 (16.2%)			
1998	471	8.0	27.9 (21.9%)	232	–19.9	31.6 (16.2%)
1999	482	6.7	28.8 (22.1%)	1825	–3.0	21.0 (12.6%)
2000	457	4.9	28.3 (21.7%)	1923	–3.0	22.0 (13.3%)
2001	521	–0.4	21.4 (15.1%)	2222	4.1	22.2 (15.2%)
2002	439	0.1	23.9 (15.8%)	3357	8.5	25.6 (17.7%)
2003	83	1.0	20.7 (15.0%)	1487	2.0	22.7 (14.7%)
2000–2003	1500	1.4	24.4 (15.4%)	8989	3.9	23.6 (15.2%)
2000–2003	No.: 10489, Bias: 3.5, RMS: 23.7 (15.5%)					

The TRITON buoys have been deployed and managed by the Japan Agency for Marine-Earth Science and Technology (JAMSTEC). The ship observations period spans April 1996 to May 2003, while the buoy observations extend from March 1998 to May 2003. Observation points used by the research vessels lay mainly in the northwest Pacific (Fig. 1(a)). It can be seen that the ship data were sampled frequently in the seas around Japan. The buoys were deposited in the western equatorial Pacific (Fig. 1(b)). Daily DSSR match-ups were made by simply averaging hourly data in one day when there were more than 6 hourly match-ups in a day within a 3° × 3° box. The temporal distribution of the daily in situ DSSR is shown in Table 1. It should be noted that the hourly in situ DSSR data from 1997–1999 were used for re-tuning the DSSR model coefficients (Kawai and Kawamura, 2005).

In the present study, NCEP/NCAR 1, ERA40 and JRA25 DSSRs in 2000 are compared with the satellite data. Basic descriptions of the satellite DSSR and the reanalysis DSSRs are shown in Table 1. ERA40 and JRA25 DSSR have the same resolution 2.5° × 2.5° grids and are available four times (00, 06, 12, 18 Z) daily. Since ERA40 provides 6-hourly integrated values, we converted to flux by dividing by integration time. JRA25 and ERA40 daily mean flux was obtained by averaging data from four periods. NCEP/NCAR 1 provides daily DSSR data with a Gaussian grid system (192 × 92 grids) the spatial resolution of which is about 180 km. Therefore, the NCEP/NCAR 1 DSSR has been interpolated into 2.5° × 2.5° grids, to conform to the spatial resolution of ERA40 and JRA25. We then sampled the three reanalysis DSSRs corresponding to the region of satellite DSSR coverage (80°E to 160°W, 60°S to 60°N) for comparison. For this purpose, the satellite DSSR is also spatially averaged in corresponding grids.

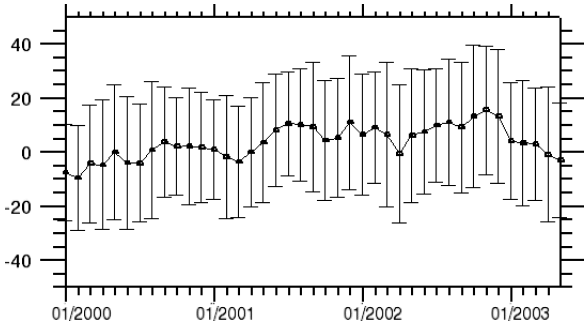

Fig. 3. Monthly bias and standard deviations of satellite DSSR errors compared with buoy DSSR in the tropics. Unit is in W/m^2. Black dots indicate monthly bias and error bars denote standard deviations of all biases in one month.

3. Comparison of the Satellite and In Situ DSSRs

3.1 Validation

The long-term high-resolution satellite DSSRs are validated using the high-quality in situ DSSRs from various aspects. First, the hourly satellite DSSRs were matched up with the in situ observations in a 0.05° × 0.05° bin. Then, through simple averaging for a day, we got daily mean match-ups. Because the in situ data during 1997–1999 were used for re-tuning the DSSR model coefficient (Kawai and Kawamura, 2005) and there were only a few match-ups in 1996, we show comparison results of the daily match-ups from January 2000 to May 2003 for ship and buoy separately (Figs. 2(a) and (b)). A good agreement between the satellite and in situ DSSRs can clearly be seen. In this period, the biases (mean of errors) ± RMS errors of the satellite DSSR have been

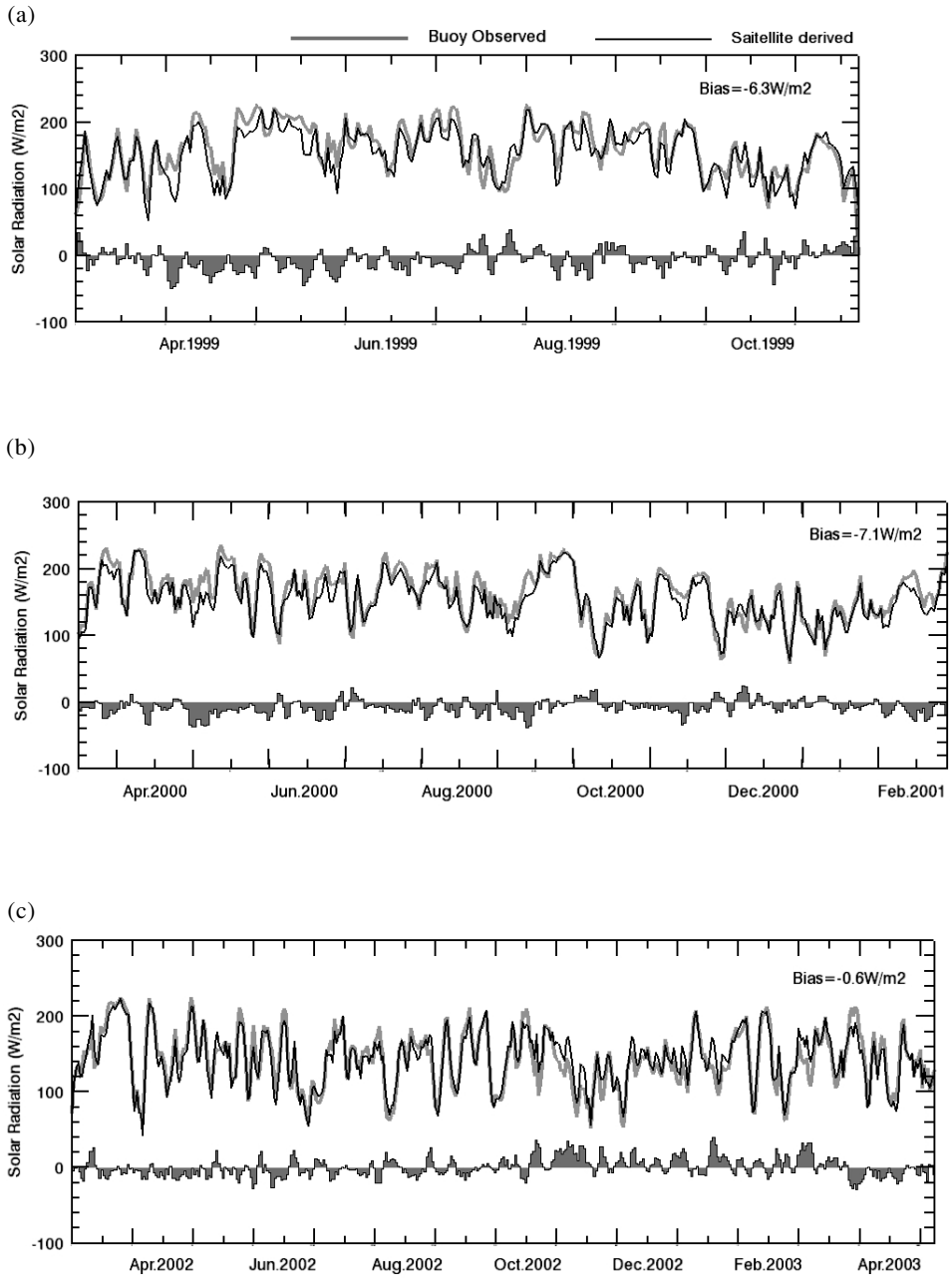

Fig. 4. Time sequences of satellite DSSR, buoy DSSR and satellite DSSR error. Buoy location is circled in Fig. 1(b) with "A" mark. (a) March 1999–December 1999, (b) March 2000–March 2001 and (c) March 2002–May 2003. Unit is W/m^2. Black line indicates the satellite DSSR and gray line indicates the buoy DSSR. Histogram indicates the bias between satellite DSSR and buoy DSSR.

found to be 1.4 ± 24.4 W/m^2 against the ship data, and 3.9 ± 23.6 W/m^2 against the buoy data, respectively. The mean and standard deviation of the satellite DSSRs within each 10 W/m^2 bin of the in situ DSSR are shown in Fig. 2(c) (ship) and Fig. 2(d) (buoy). Mean values agree very well with in situ data in each bin. Standard deviations are within 20 W/m^2.

Table 2 shows the error statistics of daily mean satellite DSSR for each year. For the whole period (1996–2003), the satellite DSSR has an accuracy of 2.6 ± 23.9 W/m^2. The RMS error is 15.5% of the daily mean in situ DSSR value. The bias and RMS error against the ship

data for 1996 and those against the buoy data for 1998 are larger because of a shortage of match-ups. Except for these cases, the bias in each year is within ±10 W/m^2 and RMS error is within 30 W/m^2.

Figure 3 shows the long-term variation of the monthly satellite DSSR errors against the buoy observations from January 2000 to May 2003 in the tropics. In most months the biases are less than 10.0 W/m^2, while the bias is larger (around 15.0 W/m^2) only in the late 2002. The reason for this is unclear. The standard deviations of the errors are always within 30.0 W/m^2. A slight seasonal variation of bias can be found in Fig. 3. In boreal winter and spring, the bias tended to be negative or smaller than the annual mean, while it becomes positive or larger in summer and autumn. Since the buoy observations are located around equatorial regions, we suppose that seasonal cloud-belt variation is the main reason (result from the ITCZ seasonal motion) underlying such slight seasonal variation.

3.2 Satellite-DSSR detectable temporal variability

The TRITON buoy moored at 156°E, 8°N (point A in Fig. 1(b)) provided time series of DSSR from March 1999 to December 1999, March 2000 to March 2001, and March 2002 to May 2003. These three one-year time sequences of the satellite and the TRITON-buoy DSSRs are shown in Fig. 4. In general, the temporal variations of satellite DSSR agree well with those of the buoy DSSR. Figures 4(a) and (b) show that the satellite DSSR tends to underestimate the buoy DSSR slightly in these two years. The biases in these years are –6.3 W/m^2 and –7.1 W/m^2, respectively, though the bias in Fig. 4(c) is –0.6 W/m^2. The errors of the satellite DSSR, indicated in Fig. 4, show that their variation range is about ±50 W/m^2 (RMS is about 20 W/m^2, see Table 1) and they have dominant variations with periods of about 5–20 days. The reasons for the short-period variability in the errors are unknown, but they may be attributed to measurement noise in the satellite and in situ sensors and atmospheric effects within the satellite grids (sub-grid problem). Further research into the DSSR retrieval scheme including the satellite/in situ sensors' characteristics and the algorithm are needed, but they are beyond the scope of present study.

4. Comparison between the Satellite DSSR and the NCEP/NCAR 1, JRA25 and ERA40 Reanalysis DSSR Products

Based on the accuracy and the temporal/spatial characteristics of satellite DSSR given in Section 3, it is used as truth reference to examine the reanalysis DSSRs. Kistler *et al*. (2001) have speculated that satellite estimates of surface net shortwave radiation might be more reliable than other global estimates of surface net shortwave radiation.

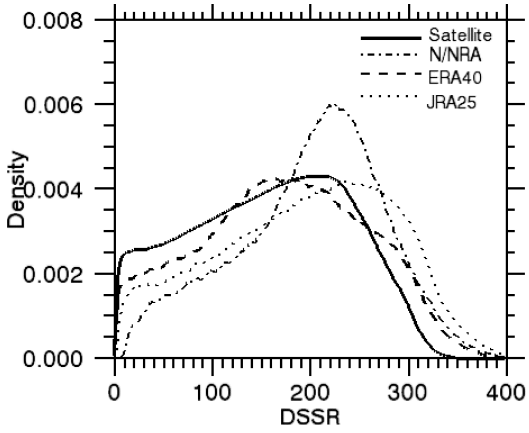

Fig. 5. Probability density function of satellite DSSR, NCEP/NCAR 1, ERA40 and JRA25 reanalysis DSSR in 2000. Unit is W/m^2.

Probability density functions (PDF) of the daily satellite DSSR, JRA25, ERA40, and NCEP/NCAR 1 over sea grids for 2000 are shown in Fig. 5. Obvious differences occur in their lower ranges from 0 to 100 W/m^2. The satellite DSSR density is higher than the reanalysis DSSRs in this range, which suggests that they may not capture lower DSSR conditions over the oceans. Among the four DSSR datasets, NCEP/NCAR 1 has the lowest probability density for the range, while in the intermediate range from 180 to 270 W/m^2, NCEP/NCAR 1 has the highest density, which results in a sharp PDF peak at around 220 W/m^2. The PDF differences in the higher range (>300 W/m^2) show that JRA25 exhibits a larger number of higher DSSR values than those of the other datasets. In the highest DSSR range, ERA40 and NCEP/NCAR 1 datasets have nearly the same probability density and both have a higher density than that of the satellite DSSR. In general, all the reanalysis datasets have lower density in the low range (<100 W/m^2) and higher density in the high range (>270 W/m^2) than that of the satellite DSSR.

Daily mean, area averaged satellite DSSR for each corresponding reanalysis grid have been prepared and then the reanalysis and satellite DSSRs in the same grid and the same day are compared directly. Mean and standard deviations of the reanalysis DSSRs within each 10 W/m^2 bin of the satellite DSSR have been calculated and are indicated in Fig. 6. Concerning the validation results shown in Section 3, we may be able to use the satellite DSSR as a standard. NCEP/NCAR 1 DSSR is overestimated in the satellite DSSR range from 0 to 260 W/m^2, while it is underestimated in the range from 260 to 360 W/m^2. ERA40 DSSR is also overestimated in the range from 0 to 220 W/m^2, but agrees with the satellite DSSR in the range from 220 to 360 W/m^2. JRA25 DSSR is over-

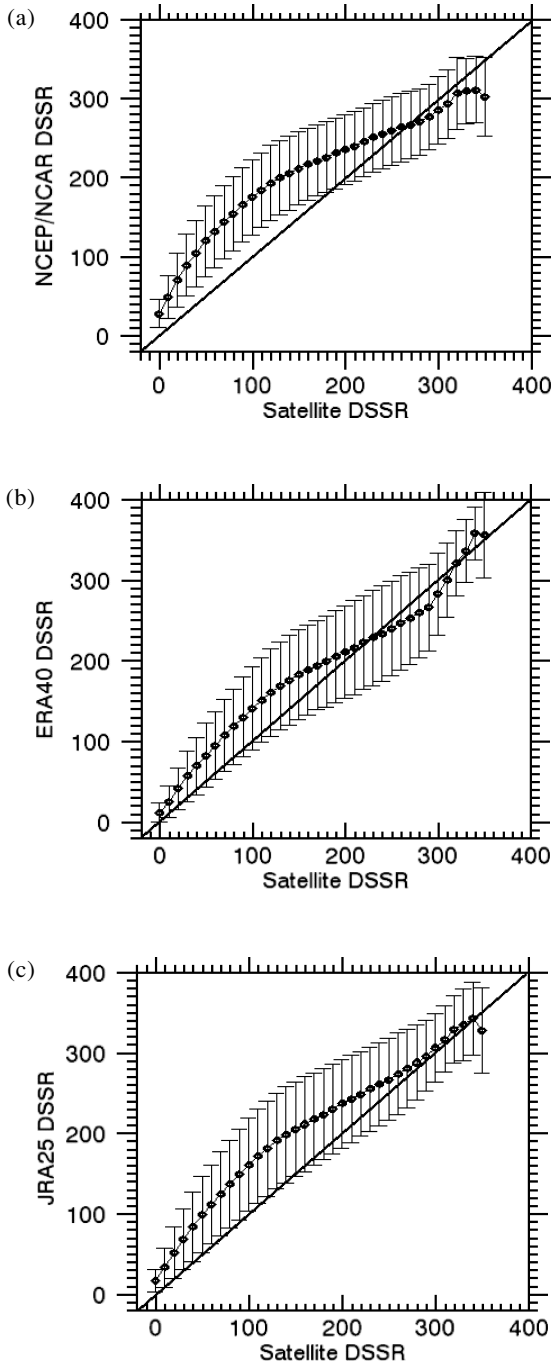

Fig. 6. Mean reanalysis DSSR value and standard deviations for 10 W/m^2 satellite DSSR bins. Error bars denote the reanalysis standard deviations of the satellite DSSR for each bin. (a) NCEP/NCAR 1, (2) ERA40, (3) JRA25. Unit is W/m^2.

estimated in the range from 0 to 270 W/m^2, and has good agreement in the range from 270 to 350 W/m^2.

To examine the spatial characteristics of the reanalysis DSSR products, correlation coefficients between the reanalysis DSSRs and the satellite DSSR have been calculated at each ocean grid for 2000 using the DSSR time series prepared for the above mentioned direct comparison (Figs. 7(a), (b) and (c)). It is seen that the correlations are low in the tropical zone, especially around the Maritime continent. The correlation coefficients increase away from the equatorial zone. JRA25 and ERA40 have better correlations with satellite data in the tropics than the NCEP/NCAR 1.

Correlation coefficients between the reanalysis DSSRs have also been calculated. As expected from the above mentioned results, the correlations are low in the equatorial zone and high in the higher latitudes (figures not shown). The correlation between JRA25 and ERA40 DSSRs is higher than those between NCEP/NCAR 1 and JRA25/ERA40.

5. Discussion

Among the reanalysis DSSR products examined here, NCEP/NCAR 1 DSSR has the largest bias of 40–60 W/m^2 in the low satellite DSSR range, and ERA40 DSSR is closer to the satellite DSSR over the whole range (Fig. 6). Its biases against the satellite DSSRs are within 30 W/m^2. Scott and Alexander (1999) have compared NCEP/NCAR 1 and ERA net shortwave fluxes with satellite data and showed that in a low-level stratiform cloud region (over extra-tropical ocean), the reanalysis net surface shortwave fluxes exhibit a positive bias, while the bias is negative in cumuliform clouds and cloud free region. The reasons for these biases could be that the satellite DSSR reflects cloud properties better than the reanalysis ones (Liu *et al.*, 2005).

According to the NCEP/NCAR Reanalysis 1 total cloud cover data (not shown) its annual maxima are over the tropical convective zones, especially over the Maritime continent (Weare, 1997). It is quite possible that the geostationary satellite observations with high temporal/spatial resolutions have great potentials for capturing cloud behavior in the cloudy tropical zones.

Among the three reanalysis DSSRs, JRA25 and ERA40 have better correlation with the satellite one than NCEP/NCAR 1 in the tropics. Scott (1999) pointed out that in winter the ERA40 shortwave fluxes have more realistic variability over the tropical oceans than the NCEP/NCAR 1. The JRA25 Working Group (2001) mentioned that, in competition with NCEP/NCAR 1 in terms of quality, the target of JRA25 is to depict the positions of tropical disturbance correctly and to describe the Asian climate accurately.

Relatively low coefficients (0.6–0.8) are found along 40°N for NCEP/NCAR (Fig. 7(a)) and JRA25 (Fig. 7(b)). Dale (1995) pointed out the large discrepancies in the summer mid-latitude regions between the NCAR CCM2 and satellite monthly mean DSSR data. He further indi-

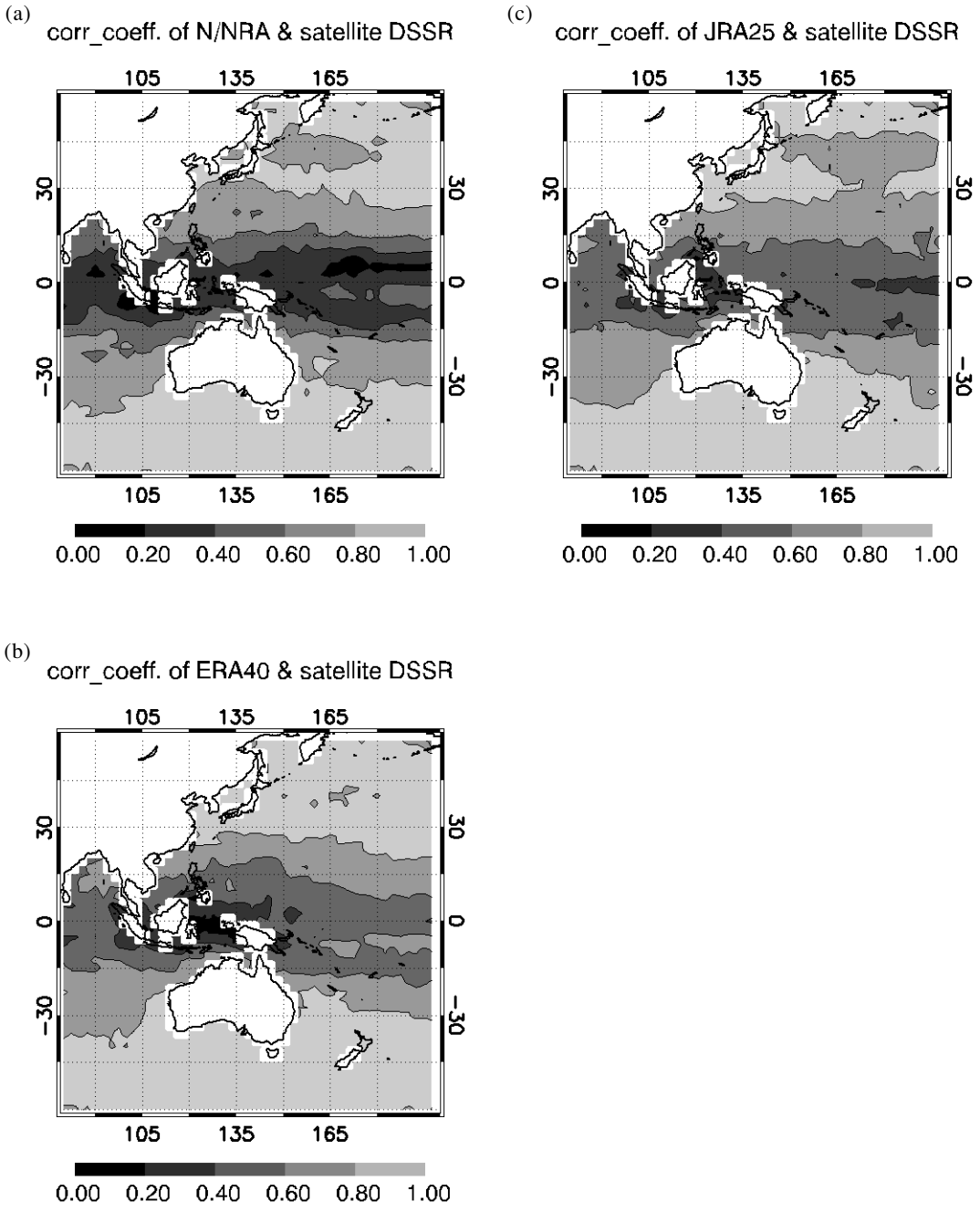

Fig. 7. Correlation coefficient between each two DSSR dataset in 2000. (a) Satellite DSSR and NCEP/NCAR1, (b) satellite DSSR and ERA40, (c) satellite DSSR and JRA25. Note higher correlation away from the equator.

cated that most of the differences are associated with cloud optical properties and cloud amount. It is well recognized that the region is frequently covered by low-level clouds during May–August, which becomes a reason for cold summers when advected to the Japanese islands (e.g., Ninomiya and Mizuno, 1985; Kawamura, 1995). The relatively low correlation might be related to the regional low-level clouds, which is left for future studies.

In summary, ERA40 and JRA25 DSSRs are closer to the satellite DSSR than NCEP/NCAR 1 DSSR. Bony *et al.* (1997) pointed out that the biases in the surface radiation fluxes derived from the NCEP reanalysis are primarily due to incorrect shortwave cloud radiative forcing and, to a lesser degree, due to a deficit in the total precipitable water and a cold bias at lower tropospheric temperature. We also note that DSSR is classified as class

C variable in the NCEP/NCAR table, indicating that it is influenced by model physics and not by observations (Kalnay *et al*., 1996).

6. Conclusions

The satellite-derived high-resolution long-term solar radiation dataset is examined for applications to research into the air-sea interaction covering different scales. First, validation of the satellite DSSR with the in situ observations was carried out. The daily mean DSSR data has high accuracy with bias ± RMS errors is 2.6 ± 23.9 W/m^2. It has been demonstrated that the temporal variability of the satellite DSSR agree well with that of the buoy-observed DSSR through comparison between their time series.

Compared with the NCEP/NCAR 1, ERA40 and JRA25 reanalysis DSSRs, the satellite DSSR dataset has higher probability density in the low value range (<100 W/m^2) and lower density in the high value range (>270 W/m^2). In particular, the overestimation of reanalysis DSSR is significant in the low DSSR range. In our Investigation of correlations between the reanalysis DSSRs and the satellite DSSR, we found that the correlation is relatively low in the tropics and becomes high away from the equator. The reanalysis DSSR temporal variations agree with those from the satellite in the high latitudes, though not in tropics.

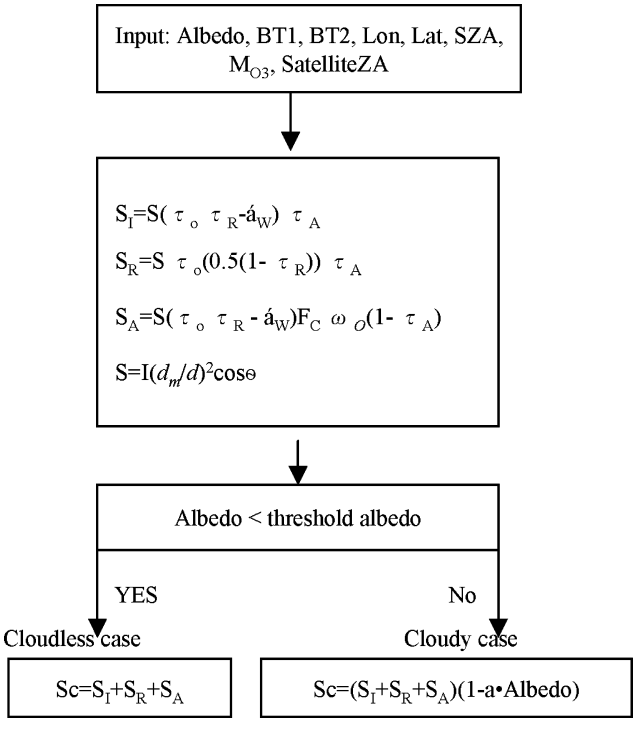

Fig. A1. Schematic diagram of the DSSR model.

Acknowledgement

We would like to express our great appreciation to the Japan Meteorological Agency and the Japan Agency for Marine-Earth Science and Technology for providing us with in situ observation data. The NCEP/NCAR Reanalysis data were provided by the NOAA-CIRES Climate Diagnostics Center, Boulder, Colorado, USA, from their web site at http://www.cdc.noaa.gov/. The JRA25 Reanalysis data were provided from the cooperative research project of the JRA-25 long-term reanalysis by Japan Meteorological Agency (JMA) and Central Research Institute of Electric Power Industry (CRIEPI). The data are provided on their web site at http://www.jreap.org/indexe.html. The ERA40 Reanalysis data were provided by European Center for Medium-Range Weather Forecasts, from their web site at http://data.ecmwf.int/data/d/era40_daily/.

This study is supported by Category 7 of MEXT (Ministry of Education, Culture, Sports, Science and Technology) RR2002 Project for Sustainable Coexistence of Human, Nature and the Earth, and by the special coordination fund for promoting science and technology under "New Generation Sea Surface Temperature" of MEXT, Japan. We appreciate Dr. Luis Albarino for improving the English of this manuscript.

Appendix: Model Description

The flow chart for production of the satellite DSSR is shown in Fig. A1. The parameters used in the model are listed in Table A1. We first input the satellite-observed

Table A1. Parameters used in the model for DSSR estimation.

BT1:	brightness temperature of the infrared-1 channel
BT2:	brightness temperature of the infrared-2 channel
Lon:	longitude in each pixel
Lat:	latitude in each pixel
SZA:	solar zenith angle
M_{O3}:	total amount of ozone
SatelliteZA:	satellite zenith angle
a:	insolation attenuation coefficient by cloud
S_I:	direct irradiance
S_R:	diffuse irradiance due to Rayleigh scattering
S_A:	diffuse irradiance due to scattering by aerosols
S:	solar radiation at the top of the atmosphere
Sc:	solar radiation at the surface
τ_o:	transmittance due to absorption by ozone
τ_R:	transmittance due to rayleigh scattering
τ_A:	transmittance due to attenuation by aerosols
α_w:	absorptance of water vapor
F_c:	ratio of forward to total scattering by aerosols
ω_o:	single scattering albedo
d_m:	sun-earth distance (annual mean)
d:	sun-earth distance

albedo, brightness temperature and satellite zenith angle, amount of ozone, latitude, longitude, time and date to the parametric model to produce the direct irradiance and diffuse irradiance due to Rayleigh scattering as well as due to scattering by aerosols. Next, the sky condition is judged using threshold albedo, which is set to a minimum of the long-term records of the observed albedo. If the albedo is equal to or less than the threshold value (cloudless case, Fig. A1), the DSSR equals the sum of direct and diffuse irradiance. If the albedo is larger than the threshold value (cloudy case), the DSSR equals the sum of direct and diffuse irradiance multiplied by the attenuation coefficient. The details of the model and the product are explained in Kawai and Kawamura (2005).

References

Bony, S., Y. Sud, K. M. Lau, J. Susskind and S. Saha (1997): Comparison and satellite assessment of NASA/DAO and NCEP/NCAR reanalysis over tropical ocean: atmospheric hydrology and radiation. *J. Climate*, **10**, 1441–1462.

Dale, M. W (1995): Comparison of the surface solar radiation budget derived from satellite data with the simulated by NCAR CCM2. *J. Climate*, **8**, 2824–2842.

Gautier, C., G. Diak and S. Masse (1980): A simple physical model to estimate incident solar radiation at the surface from GOES satellite data. *J. Appl. Meteor.*, **19**, 1005–1012.

Hanawa, K. and S. Kizu (1990): In situ measurements of solar radiation over the sea south of Japan. *J. Meteor. Soc. Japan*, **68**, 607–611.

Iwasaka, N., S. Kuwashima, H. Otobe, K. Hanawa, H. Hagiwara and R. Suzuki (1994): *In situ* measurement of incoming solar radiation by voluntary ships in the western Pacific. *J. Oceanogr.*, **50**, 713–723.

JRA 25 Working Group (2001): Japanese 25-year Reanalysis Plan, http://www.jreap.org/publications/plan/jra25plan_e.pdf

Kalnay, E., M. Kanamitsu, R. Kistler, W. Collins, D. Deaven, L. Gandin, M. Iredell, S. Saha, G. White, J. Woollen, Y. Zhu, A. Leetmaa, B. Reynolds, M. Chelliah, W. Ebisuzaki, W. Higgins, J. Janowiak, K. C. Mo, C. Ropelewski, J. Wang, R. Jenne and D. Joseph (1996): The NCEP/NCAR 40-year reanalysis project. *Bull. A. Meteorol. Soc.*, **77**, 437–471.

Kanamitsu, M., W. Ebisuzaki, J. Woolen, J. Potter and M. Fiorino (2002): NCEP/DOE AMIP-II Reanalysis (R-2). *Bull. A. Meteorol. Soc.*, **83**, 1631–1634.

Kawai, Y. and H. Kawamura (2005): Validation and improvement of satellite-derived surface solar radiation over the northwestern Pacific Ocean. *J. Oceanogr.*, **61**, 79–89.

Kawamura, H. (1995): Yamase and its remote sensing. In *Yamase*, ed. by H. Kawamura, *Meteorological Research Note*, **183**, 153–179.

Kawamura, H., T. Tanahashi and T. Takahashi (1998): Estimation of insolation over the Pacific Ocean off the Sanriku coast. *J. Oceanogr.*, **54**, 457–464.

Kiehl, J. T. and K. E. Trenberth (1997): Earth's annual global mean energy budget. *Bull. A. Meteorol. Soc.*, **78**, 197–207.

Kistler, R., E. Kalnay, W. Collins, S. Saha, G. White, J. Woollen, M. Chelliah, W. Ebisuzaki, M. Kanamitsu, V. Kousky, H. Dool, R. Jenne and M. Fiorino (2001): The NCEP-NCAR 50-year reanalysis: monthly means CD-ROM. *Bull. A. Meteorol. Soc.*, **82**, 247–267.

Kizu, S. (1995): A study on thermal response of ocean surface layer to solar radiation using satellite remote sensing. Doctoral Thesis, Tohoku Univ. Sendai, Japan, 100 pp.

Liu, J., J. A. Curry, W. B. Rossow, J. R. Key and X. Wang (2005): Comparison of surface radiative flux data sets over the Arctic Ocean. *J. Geophys. Res.*, **110**, C02015, doi:10.1029/2004JC002381.

Ninomiya, K. and H. Mizuno (1985): Anomolous cold spell in summer over northeastern Japan caused by northeasterly wind from polar maritime air-mass. Part-I: EOF analysis of temperature variation in relation to the large-scale situation causing the cold summer. *J. Meteor. Soc. Japan*, **63**, 845–857.

Scott, J. D. and M. A. Alexander (1999): Net shortwave fluxex over the ocean. *J. Phys. Oceanogr.*, **29**, 3167–3174.

Tanahashi, S., H. Kawamura, T. Matsuura, T. Takahashi and H. Yusa (2000): Improved estimates of hourly insolation from GMS S_VISSR data. *Remote Sens. Environ.*, **74**, 409–413.

Tanahashi, S., H. Kawamura, T. Matsuura, T. Takahashi and H. Yusa (2001): A system to distribute satellite incident solar radiation in real-time. *Remote Sens. Environ.*, **75**, 412–422.

Weare, B. C. (1997): Comparison of NCEP-NCAR cloud radiative forcing reanalyses with observations. *J. Climate*, **10**, 2200–2205.

Webster, P. J. and R. Lukas (1992): TOGA COARE: The coupled ocean-atmosphere response experiment. *Bull. A. Meteorol. Soc.*, **73**, 1377–1414.

Zhang, Y., W. B. Rossow, A. A. Lacis, V. Oinas and M. I. Mishchenko (2004): Calculation of radiative fluxes from the surface to top of atmosphere based on ISCCP and other global data sets: Refinements of the radiative transfer model and the input data. *J. Geophys. Res.*, **109**, D19105, doi:10.1029/2003JD004457.